Earthq Eng & Eng Vib (2016) 15: 715-727 **DOI**:10.1007/s11803-016-0360-y

Dynamic soil-tunnel interaction in layered half-space for incident plane SH waves

Fu Jia[1,2†], Liang Jianwen[1,2‡] and Qin Lin[2§]

1. *State Key Laboratory of Hydraulic Engineering Simulation and Safety, Tianjin University, Tianjin 300354, China*

2. *Department of Civil Engineering, Tianjin University, Tianjin 300354, China*

Abstract: The dynamic soil-tunnel interaction is studied by indirect boundary element method (IBEM), using the model of a rigid tunnel in layered half-space, which is simplified to a single soil layer on elastic bedrock, subjected to incident plane SH waves. The accuracy of the results is verified through comparison with the analytical solution. It is shown that soil-tunnel interaction in layered half-space is larger than that in homogeneous half-space and this interaction mechanism is essentially different from that of soil-foundation-superstructure interaction.

Keywords: underground tunnel; layered half-space; plane SH wave; indirect boundary element method; soil-tunnel interaction; site dynamic characteristics

1 Introduction

The dynamic response of underground tunnels to seismic excitation is a fundamental problem in the earthquake analysis of infrastructure. In the past decades, scholars generally used two groups of methods− analytical and numerical − to study this problem. Wave function expansion technique is a widely used analytical method; it employs infinite series sum to simulate the scattered field aroused by tunnels to satisfy different boundary conditions. Although it can only solve linear-elastic problems and simple-shaped tunnels, it is very useful to explore the physical nature and check the accuracy of numerical methods. The dynamic response of underground tunnels to out-of-plane waves (Lee and Trifunac, 1979) and to in-plane waves (Liang *et al*., 2005a, b) in homogeneous half-space have been obtained by this technique. The solution was also extended to group tunnels (Balendra *et al*., 1984) and to tunnels in fluid-saturated medium (Hasheminejad and Avazmohammadi, 2008).

Numerical methods, such as finite element method (FEM) and boundary element method (BEM), are better suited for studying more complex problems, e.g., arbitrary-shaped tunnels, non-linear characteristics, three-dimensional geometry, and complex site conditions. For example, an arc-shaped tunnel was studied by analyzing the dynamic displacement and stress distributions at the soil-structure interface (Wong *et al*., 1985). Non-linear interaction between a tunnel and its surrounding soil was studied by comparing the difference in damage evolutions between the tunnel liner and soil cavity (Hatzigeorgiou and Beskos, 2010). The three-dimensional response of a tunnel embedded in a horizontally layered half-space to the excitation of harmonic body waves was obtained, and the ground surface displacement was studied (Luco and De Barros, 1994, De Barros and Luco, 1994). More recently, the influence of local topography, such as a canyon or hill, (Parvanova *et al*., 2014), and above-ground structures (Pitilakis *et al*., 2014) on tunnel dynamic responses was discussed.

As underground concrete tunnels or precast concrete culverts or pipes are much stiffer than the surrounding soil, they generally behave as rigid objects in the axial direction, and it is reasonable to model them as rigid body. However, there are limited studies on the problem of soil-tunnel interaction, especially the role of site dynamic characteristics. In this paper, we use the model of a rigid tunnel embedded in layered half-space to incident plane SH waves to study the site effect on dynamic soil-tunnel interaction. The layered half-space is simplified to a single layer on bedrock, and the tunnel is assumed to be completely embedded within the soil layer for convenience. In a companion paper we use

Correspondence to: Liang Jianwen, State Key Laboratory of Hydraulic Engineering Simulation and Safety, Tianjin University, Tianjin 300354, China
Tel: +86-22-27404025; Fax: +86-22-27404025
E-mail: liang@tju.edu.cn
†PhD candidate; ‡Professor; §Undergraduate

Supported by: National Natural Science Foundation of China under Grant 51378384 and Key Project of Natural Science Foundation of Tianjin Municipality under Grant 12JCZDJC29000.

Received February 27, 2015; **Accepted** August 24, 2015

the same model to in-plane excitation to study the soil-tunnel interaction further.

The numerical method employed in this paper is indirect boundary element method (IBEM), a kind of BEM that uses fictitious loads as the unknowns. The accuracy of the results is high and it agrees well with the results by analytical methods. It should be pointed out that although the layered half-space is simplified into a single layer on elastic bedrock and the tunnel of circular cross-section is taken as example, the method described in this paper can be applied to more general problems with multi-layered half-spaces and other tunnel shapes.

2 Methodology

2.1 Model

As shown in Fig. 1, an underground tunnel of circular cross-section is completely rigid with outer radius a and mass M_0 per unit length. The boundary between the tunnel and its surrounding soil is marked as Γ, and it is assumed that there is no slippage on Γ. The embedded depth from ground surface to the tunnel center is d. The layered half-space is simplified to a single layer on bedrock. Both the soil layer and bedrock are elastic, homogeneous and isotropic medium. The material parameters of the bedrock are characterized by shear wave velocity β_R, mass density ρ_R, shear modulus μ_R and damping ratio ζ_R, while the soil layer is of thickness D, its material parameters are characterized by shear wave velocity β_L, mass density ρ_L, shear modulus μ_L and damping ratio ζ_L. The harmonic plane SH wave is incident from depth D' with horizontal angle θ and circular frequency ω. The complex material constants β and μ denoted by superscript * are obtained by the correspondence theory

$$\beta^* = \beta\sqrt{1+2\mathrm{i}\xi} \tag{1a}$$

$$\mu^* = \mu\left(1+2\mathrm{i}\xi\right) \tag{1b}$$

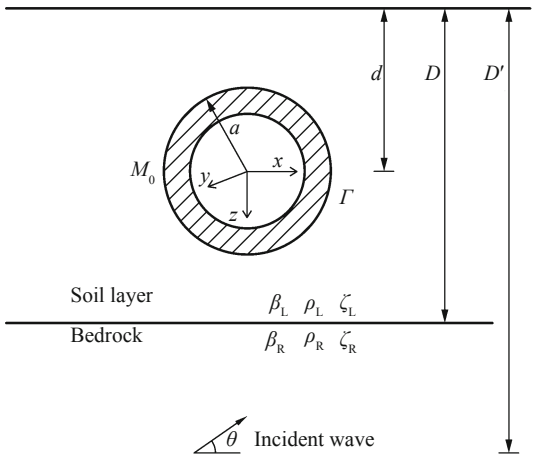

Fig. 1 Model of rigid tunnel embedded within a single layer on elastic bedrock

In order to use IBEM, the half-space from ground surface to incident location ("incident bedrock" in the following for convenience) is divided into N sub-layers, with the material constants of the nth sub-layer denoted by the subscript of n. The tunnel boundary Γ is divided into M elements of straight lines. It is better to make all elements along boundary Γ the same length, and make all sub-layers above tunnel top and under tunnel bottom the same thickness, in order that IBEM can perform best. Also, there should be more sub-layers from tunnel top to bottom than other parts of the half-space to ensure accuracy.

2.2 Free-field response

The wave number k of incident harmonic SH wave is

$$k = \frac{\omega\cos\theta}{\beta_R^*} \tag{2}$$

The stiffness matrix $\boldsymbol{E}_n$ of each sub-layer and incident bedrock E_R are

$$\boldsymbol{E}_n = \begin{bmatrix} E_n^{11} & E_n^{12} \\ E_n^{21} & E_n^{22} \end{bmatrix} = \frac{kt_n\mu_n^*}{\sin kt_nD_n}\begin{bmatrix} \cos kt_nD_n & -1 \\ -1 & \cos kt_nD_n \end{bmatrix} \quad (n = 1, 2, \ldots, N) \tag{3a}$$

$$E_R = \mathrm{i}kt_R\mu_R^* \tag{3b}$$

where $\mathrm{i} = \sqrt{-1}$ is the imaginary unit, D_n is the thickness of nth sub-layer, t_n and t_R are related to the incident angle

$$h_R = \cos\theta,\ \ t_R = -\mathrm{i}\sqrt{1-1/h_R^2} \tag{4a}$$

$$h_n = \beta_n^* h_R / \beta_R^*,\ t_n = -\mathrm{i}\sqrt{1-1/h_n^2} \tag{4b}$$

The stiffness matrix of the site $\boldsymbol{S}$ is formed by merging $\boldsymbol{E}_n$ and E_R into a matrix

$$\boldsymbol{S} = \begin{bmatrix} E_1^{11} & E_1^{12} & & & & \cdots & \\ E_1^{21} & E_1^{22}+E_2^{11} & E_2^{12} & & & & \\ & E_2^{21} & E_2^{22}+E_3^{11} & E_3^{12} & & & \vdots \\ & & E_3^{21} & E_3^{22}+E_4^{11} & & & \\ \vdots & & & & \ddots & & \\ & & & & & E_N^{11}+E_{N-1}^{22} & E_N^{12} \\ & \cdots & & & & E_N^{21} & E_N^{22}+E_R \end{bmatrix} \tag{5}$$

The out-of-plane tractions on the interfaces of all sub-layers is $\boldsymbol{Q} = \{0, 0, \ldots, 0, Q_R\}^T$, with all elements being 0 except the last one caused by incident wave with amplitude v_{SH}

$$Q_R = E_R v_{SH} \tag{6}$$

Then the vector $\boldsymbol{V}=\{v_1, v_2, \dots, v_N, v_{N+1}\}^{\mathrm{T}}$ representing the interface displacements of all sub-layers can be obtained by

$$\boldsymbol{SV}=\boldsymbol{Q} \tag{7}$$

The displacement $v(z)$ of wave-number domain in the nth sub-layer is

$$v(z)=A_{\mathrm{SH}}\exp(\mathrm{i}kt_n z)+B_{\mathrm{SH}}\exp(-\mathrm{i}kt_n z) \tag{8}$$

where two unknown coefficients A_{SH} and B_{SH} can be determined from two boundary conditions v_n (z = 0) and v_{n+1}($z=D_n$). Then the displacement $v(x, z)$ and out-of-plane traction $\tau(x, z)$ of space domain at point (x, z) within this sub-layer are

$$v(x,z)=\left[A_{\mathrm{SH}}\exp(\mathrm{i}kt_n z)+B_{\mathrm{SH}}\exp(-\mathrm{i}kt_n z)\right]\exp(-\mathrm{i}kx)\exp(\mathrm{i}\omega t) \tag{9a}$$

$$\tau(x,z)=\mathrm{i}kt_n\mu_n^*\left[A_{\mathrm{SH}}\exp(\mathrm{i}kt_n z)-B_{\mathrm{SH}}\exp(-\mathrm{i}kt_n z)\right]\exp(-\mathrm{i}kx)\exp(\mathrm{i}\omega t) \tag{9b}$$

Also, the displacement and traction at point (x', z') within incident bedrock are

$$v(x',z')=B'_{\mathrm{SH}}\exp(-\mathrm{i}kt_{\mathrm{R}}z')\exp(-\mathrm{i}kx')\exp(\mathrm{i}\omega t) \tag{10a}$$

$$\tau(x',z')=-\mathrm{i}kt_{\mathrm{R}}\mu_{\mathrm{R}}^* B'_{\mathrm{SH}}\exp(-\mathrm{i}kt_{\mathrm{R}}z')\exp(-\mathrm{i}kx')\exp(\mathrm{i}\omega t) \tag{10b}$$

where the unknown coefficient B'_{SH} can be determined from boundary condition v_{N+1} (z' = 0). Further details on the calculation of free-field response can be found in the book by Wolf (1985).

2.3 Impedance function

In order to use IBEM, a set of fictitious out-of-plane loads $q_m e^{\mathrm{i}\omega t}$ (m=1, 2, … , M) distributed uniformly on inclined lines are applied onto the boundary Γ as shown in Fig. 2; the time factor $e^{\mathrm{i}\omega t}$ is omitted hereafter for convenience. The values of these fictitious loads are unknowns, and should be determined for the assumed boundary conditions that the tunnel produces a unit out-of-plane displacement to the excitation of these loads.

The tunnel displacement at point (x, z) on the mth element can be expressed as

$$U(x,z)=\sum_{m=1}^{M} gu_{jm}(x,z)\,q_m \qquad (x,z)\in j\text{th element} \tag{11}$$

where $gu_{jm}(x, z)$ is the displacement Green's function, meaning the out-of-plane displacement at point (x, z) of the jth element when a unit fictitious line load is imposed on the mth element. Details on the calculation of Green's functions can be founded in the book by Wolf (1985).

The no-slippage condition along boundary Γ gives that

$$U(x,z)=\sum_{m=1}^{M} gu_{jm}(x,z)\,q_m=1 \qquad (x,z)\in j\text{th element} \tag{12}$$

If M points from M elements are chosen respectively, we can obtain a set of linear equations like Eq. (12) from which q_m (m = 1, 2, … , M) can be solved. The traction along tunnel circumference is

$$T(x,z)=\sum_{m=1}^{M} gt_{jm}(x,z)\,q_m \qquad (x,z)\in j\text{th element} \tag{13}$$

where $g_{jm}(x, z)$ is the traction Green's function at point (x, z). The total force imposed onto the tunnel represents the tunnel impedance function K_{yy}, which can be obtained by integral with respect to tractions along boundary Γ

$$K_{yy}=\int_{\Gamma} T(x,z)\,\mathrm{d}s \tag{14}$$

The impedance function is related to the tunnel shape, site condition, embedment depth and harmonic frequency, but independent of tunnel mass and incident waves. Also, it is convenient to write the complex-valued impedance function K_{yy} into the following form

$$K_{yy}=\mu_{\mathrm{L}}\left(k_{yy}+\mathrm{i}\frac{\omega a}{\beta_{\mathrm{L}}}c_{yy}\right) \tag{15}$$

The real part k_{yy} represents the stiffness coefficient of the tunnel, while the imaginary part c_{yy} is the radiation damping coefficient. They are all dimensionless.

2.4 Tunnel response

The out-of-plane rigid displacement of the tunnel under the excitation of incident harmonic wave, whose amplitude is also assumed to be unit 1, can be decomposed into two parts

$$\Delta=\Delta_1+\Delta_2 \tag{16}$$

where Δ_1 is the displacement of a massless tunnel under the excitation of harmonic incident waves while Δ_2 is the additional displacement associated with inertia force F_0

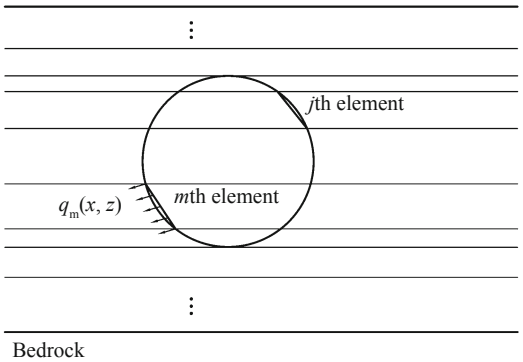

Fig. 2 Green's functions of distributed load on an inclined line

caused by its mass. Δ_1 can be obtained by the reciprocity theory (Luco, 1986),

$$\Delta_1 = \frac{\int_\Gamma [v_f(x,z)\tau(x,z) - \tau_f(x,z)]\mathrm{d}s}{K_{yy}} \tag{17}$$

with $\tau(x, z)$ being the traction at point (x, z) on boundary Γ for harmonic incident wave, $v_f(x, z)$ and $t_f(x, z)$ being the displacement and traction of free-field ground motion at point (x, z) on boundary Γ.

Based on the concept of impedance function, Δ_2 is

$$\Delta_2 = \frac{F_0}{K_{yy}} \tag{18}$$

For a rigid body

$$F_0 = \omega^2 M_0 \Delta \tag{19}$$

By introducing Eqs. (18) and (19) into Eq. (16), it becomes

$$\Delta = \frac{\Delta_1}{1 - \omega^2 M_0 / K_{yy}} \tag{20}$$

The symbol Δ is also dimensionless. In fact it can represent not only the tunnel displacement but also the amplification factor of incident excitation. Further details on the formula of dynamic response can be found in Luco and Wong (1982).

3 Verification of accuracy

A comparison between our results and an analytical solution which uses wave function expansion technique (Fu *et al*., 2016) in undamped homogeneous half-space is given in Table 1. As Fu *et al*. (2016) is in Chinese, the concise process and solution is provided in the Appendix.

Table 1 Comparison between method of this paper and analytical method by wave function expansion technique (d/a = 2, M_0/M_s=1/4)

$\omega a/\beta_L$		$\theta=5^\circ$	$\theta=30^\circ$	$\theta=60^\circ$	$\theta=90^\circ$	$\omega a/\beta_L$		$\theta=5^\circ$	$\theta=30^\circ$	$\theta=60^\circ$	$\theta=90^\circ$
0.3	①	1.886376	1.785927	1.584380	1.486457	3.3	①	0.907396	0.928843	0.46487	0.469992
	②	1.886340	1.785892	1.584356	1.486439		②	0.907126	0.928145	0.464748	0.470613
	③	**1.91(-5)**	**1.96(-5)**	**1.51(-5)**	**1.21(-5)**		③	**2.98(-4)**	**7.51(-4)**	**2.62(-4)**	**1.32(-3)**
0.6	①	1.790347	1.489649	0.944170	0.719161	3.6	①	0.813673	0.790623	0.601826	0.306946
	②	1.790284	1.489592	0.944128	0.719117		②	0.813526	0.790137	0.601691	0.307147
	③	**3.52(-5)**	**3.83(-5)**	**4.45(-5)**	**6.12(-5)**		③	**1.81(-4)**	**6.15(-4)**	**2.24(-4)**	**6.55(-4)**
0.9	①	1.651455	1.168717	0.434804	0.388342	3.9	①	0.686806	0.585754	0.612757	0.256333
	②	1.651402	1.168659	0.434758	0.388356		②	0.686750	0.585551	0.612617	0.256263
	③	**3.21(-5)**	**4.96(-5)**	**1.06(-4)**	**3.61(-5)**		③	**8.15(-5)**	**3.47(-4)**	**2.28(-4)**	**2.73(-4)**
1.2	①	1.462837	0.814242	0.206494	0.553760	4.2	①	0.508811	0.325828	0.483569	0.335670
	②	1.462771	0.814183	0.206546	0.553800		②	0.508666	0.325758	0.483541	0.335607
	③	**4.51(-5)**	**7.25(-5)**	**2.52(-4)**	**7.22(-5)**		③	**2.85(-4)**	**2.15(-4)**	**5.79(-5)**	**1.88(-4)**
1.5	①	1.199691	0.463973	0.563497	0.676321	4.5	①	0.242107	0.164175	0.207992	0.397606
	②	1.199474	0.463856	0.563395	0.676203		②	0.242104	0.164121	0.207952	0.397621
	③	**1.81(-4)**	**2.52(-4)**	**1.81(-4)**	**1.74(-4)**		③	**1.24(-5)**	**3.29(-4)**	**1.92(-4)**	**3.77(-5)**
1.8	①	0.832112	0.563969	0.948117	0.571007	4.8	①	0.228955	0.376790	0.265606	0.334713
	②	0.831776	0.563697	0.947668	0.570661		②	0.229016	0.376775	0.265584	0.334749
	③	**4.04(-4)**	**4.82(-4)**	**4.74(-4)**	**6.06(-4)**		③	**2.66(-4)**	**3.98(-5)**	**8.28(-5)**	**1.08(-4)**
2.1	①	0.736768	0.900091	0.996029	0.433675	5.1	①	0.529647	0.357105	0.574964	0.246955
	②	0.736925	0.899942	0.995578	0.433412		②	0.529920	0.357276	0.575214	0.247130
	③	**2.13(-4)**	**1.66(-4)**	**4.53(-4)**	**6.06(-4)**		③	**5.15(-4)**	**4.79(-4)**	**4.35(-4)**	**7.09(-4)**
2.4	①	0.915718	1.016313	0.686056	0.590537	5.4	①	0.551041	0.272468	0.599839	0.321502
	②	0.915861	1.017407	0.687212	0.590357		②	0.552992	0.273474	0.601949	0.322612
	③	**1.56(-4)**	**1.08(-3)**	**1.69(-3)**	**3.05(-4)**		③	**3.54(-3)**	**3.69(-3)**	**3.52(-3)**	**3.45(-3)**
2.7	①	0.988571	1.030101	0.333738	0.675426	5.7	①	0.474646	0.366251	0.509892	0.362719
	②	0.988299	1.028998	0.333798	0.676128		②	0.473161	0.365111	0.508274	0.361611
	③	**2.75(-4)**	**1.07(-3)**	**1.80(-4)**	**1.04(-3)**		③	**3.13(-3)**	**3.11(-3)**	**3.17(-3)**	**3.05(-3)**
3.0	①	0.971069	1.003711	0.266114	0.619043	6.0	①	0.383439	0.470699	0.361788	0.342319
	②	0.970782	1.002908	0.265960	0.619740		②	0.382920	0.470061	0.361293	0.341849
	③	**2.96(-4)**	**8.00(-4)**	**5.79(-4)**	**1.13(-3)**		③	**1.35(-3)**	**1.36(-3)**	**1.37(-3)**	**1.37(-3)**

Notes: ①Results of analytical method with accuracy restricted within 1×10^{-8}; ②Results by method of this paper;
③Error represented by |①-②|/①, the value 1.91(-5) means 1.91×10^{-5} for example

The embedded depth of the tunnel is d/a = 2, and its mass is M_0/M_s=1/4 with M_s being the soil replaced by the tunnel. For our method, the soil layer and the bedrock have the same material parameters and degenerate into a homogeneous half-space, and the damping ratio is set to be $\xi_R = \xi_L = 1\times10^{-5}$ to simulate undamped half-space. The bedrock location and the depth of incident wave are assumed to be $D'/a = D/a = 3$. The part of the half-space from tunnel top to bottom is divided into 400 sub-layers with every element along the tunnel boundary having the same length, while the part above the tunnel top does not need to be treated so finely, so it is divided into 100 sub-layers of the same thickness. The bedrock where the incident wave comes from does not need discretization. For wave function expansion methods, the homogeneous half-space is exactly undamped and the incident location of plane waves does not influence the results. The accuracy of the wave function expansion method is restricted within 1×10^{-8}. It is observed that the results by our method agree well with the results by analytical method with errors of no more than 4‰ in the range $0 < \omega a/\beta_L < 6$. Hence, the accuracy of our method is high.

4 Numerical results and analysis

In this chapter, the parameters of layered half-space are $\rho_R = \rho_L = 2000$ kg/m^3, $\xi_R = 0.05$, $\xi_L = 0.02$, with the ratio of the soil-layer thickness to the tunnel radius ("soil-layer thickness" for short in the following) varying with three values D/a = 4, 6, and 8, and the shear wave velocity ratio of the soil layer to the bedrock ("bedrock stiffness" for short) also varying with four values β_R/β_L = 2, 3, 5, and ∞. The mass density of the homogeneous half-space is $\rho_R = \rho_L = 2000$ kg/m^3 with damping ratio of $\xi_R = \xi_L = 0.05$. The incident wave comes from $D'/a = 8$ for all half-spaces. The embedment depth also varies with three values d/a = 1.5, 2 and 2.5, which make the tunnel embedded within the soil layer in order to study the site effect conveniently. The part of the half-space from tunnel top to bottom is divided into 180 sub-layers, and the part above tunnel top is divided into 20 sub-layers, with that from tunnel bottom to incident bedrock divided into sub-layers of the same thickness. There is no need to use as many sub-layers in this chapter as the last chapter because the damping ratio is much lager here.

4.1 Impedance function

Figure 3 is the impedance function of tunnel in frequency domain for a homogeneous half-space and layered half-space. It is observed that the real part and the imaginary part of the impedance function of both the homogeneous half-space and layered half-space are all vibrating function in frequency domain. However, the impedance function of the homogeneous half-space is relatively smooth while there are "ripples" on the spectrum of impedance function of layered half-space. For shallow embedment (d/a = 1.5) and deep embedment (d/a = 2.5), the spectrum vibrating periods of the impedance function for the homogeneous half-space and layered half-space are generally the same, and the impedance function of layered half-space fluctuates around that of the homogeneous half-space. The different D/a value and β_R/β_L value do not change the vibrating period of the impedance functions of the layered half-space, they only change the amplitude of "ripples" on the curves in the way that large D/a values and large β_R/β_L values all result in larger amplitude of "ripples". For intermediate embedment, if the soil-layer thickness is large (D/a = 6 and 8), the characteristics of impedance function are the same as the condition d/a = 1.5 and d/a=2.5, while for small soil-layer thickness (D/a = 4), the vibrating period of impedance function of layered half-space with small bedrock stiffness (β_R/β_L = 2 and 3), and that of homogeneous half-space are the same. But if bedrock stiffness is large (β_R/β_L = 5 and ∞), the vibrating period of the impedance function of the layered half-space is evidently short than that of the homogeneous half-space.

4.2 Tunnel response

Figures 4 and 5 are the spectrum of tunnel out-of-plane displacement in homogeneous half-space and layered half-space for different incident angles (q = 5°, 30°, 60° and 90°). The dimensionless tunnel mass is M_0/M_s = 1/4 and the embedment depth is d/a = 2. It is observed that for the layered half-space, the tunnel response increases with increasing incident angle for β_R/β_L = 2, 3, and 5, but it is independent of incident angle for $\beta_R/\beta_L = \infty$. Also for the layered half-space, there is an evident peak in the low frequency domain on spectrum for large incident angle (θ = 60° and 90°), and the value of this peak is larger than 2; if the bedrock stiffness is large (β_R/β_L = 5 and ∞), the peak is evident even for small incident angles (θ = 5° or θ = 30°). The situation is essentially different for homogeneous half-space: the tunnel response for very small incident angle (θ = 5°) is larger than that for other incident angles, and there is no peak on the spectrum. This is because the site dynamic characteristics of a layered half-space introduce much influence on tunnel spectrum; the homogeneous half-space does not involve these characteristics of the site.

For layered half-space, it is also noticed that the peak value increases with increasing soil-layer thickness, because the path by which the incident wave propagates and amplifies is longer in the thicker soil layer. To explain this phenomenon further, the displacement at tunnel center of free-field motion for θ = 90° is plotted in Fig. 6, in which the peak value also increases with increasing soil-layer thickness.

Figure 7 shows the tunnel displacement spectrums in homogeneous half-space and layered half-spaces for θ = 90°. The dimensionless tunnel mass varies with three values M_0/M_s=0, 1/4 and 1/2. The three numbers in each sub-figure is the peak frequency of D/a = 8, 6,

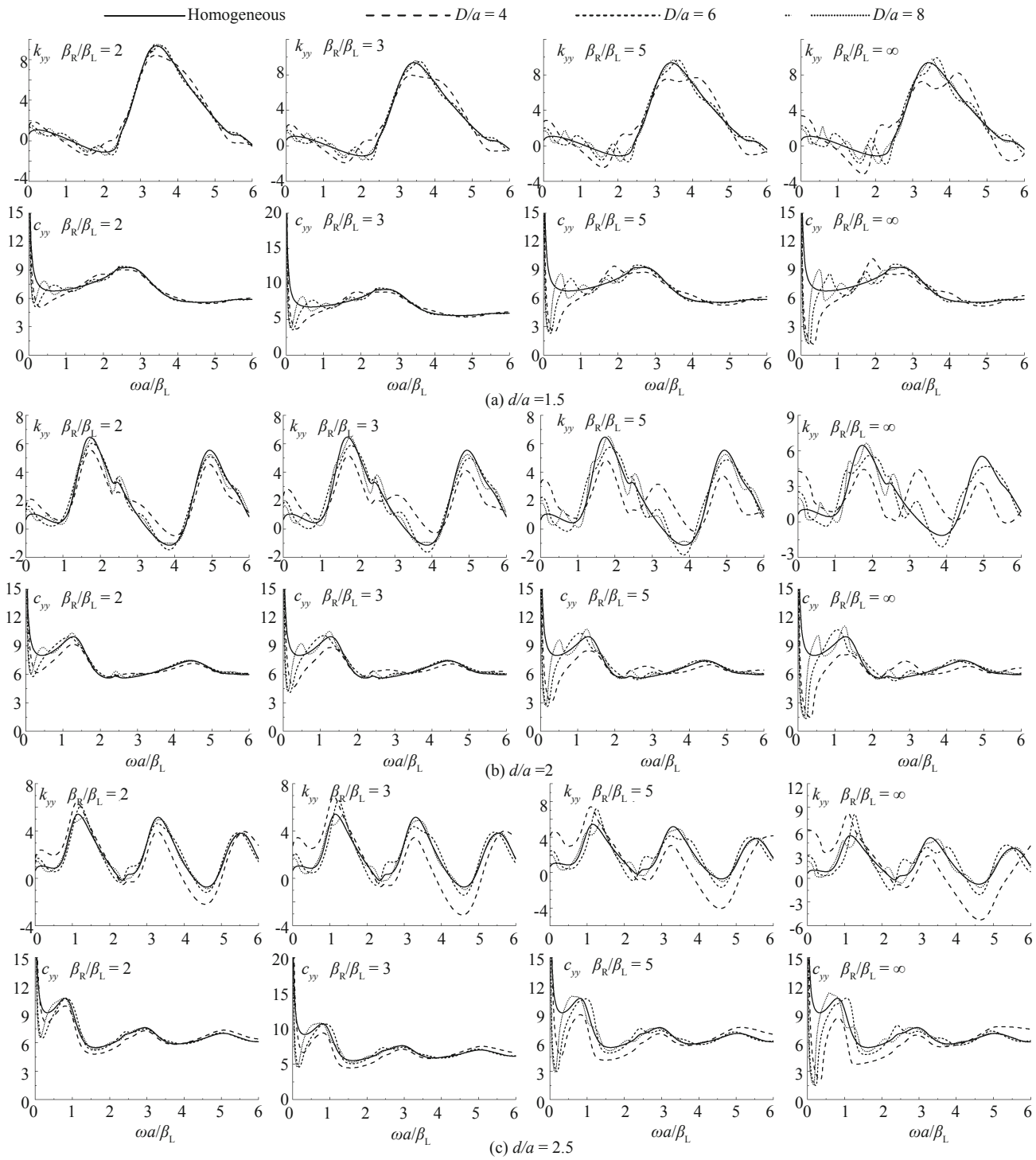

Fig. 3 Impedance function of tunnel versus different bedrock stiffness and soil-layer thickness in frequency domain ($\rho_R = \rho_L = 2000\text{kg/m}^3$, $\xi_R = 0.05$ and $\xi_L = 0.02$ for layered half-space, $\xi_R = \xi_L = 0.05$ for homogeneous half-space)

and 4, respectively; symbol *** means that the peak degenerates in this condition. The tunnel response in layered half-spaces is evidently larger than that in homogeneous half-space. This is also because the layered half-space involves the site dynamic characteristics while the homogeneous half-space does not include these characteristics.

For free-field response in layered half-space, the frequencies for which interference produces maximum response of the soil layer (resonant frequencies) are

$$\omega_L = \frac{(2j-1)\pi\beta_L}{2D} \quad (j = 1,2,3\ldots) \tag{21}$$

So D/a = 4 corresponds to dimensionless resonant frequencies $\omega_L a/\beta_L$ =0.39, 1.18, 1.96, … , D/a = 6 corresponds to $\omega_L a/\beta_L$ = 0.26, 0.79, 1.31, … , D/a = 8 corresponds to $\omega_L a/\beta_L$ = 0.20, 0.59, 0.98, … and so on. It is noticed that the peak frequency of the tunnel response ω_{peak} evidently becomes lower with increasing soil-layer

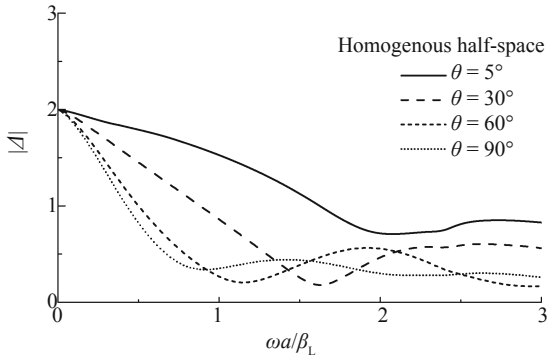

Fig. 4 The spectrum of tunnel displacement versus incident angle θ in homogeneous half-space (d/a=2, $\rho_R = \rho_L$= 2000 kg/m^3, $\xi_R = \xi_L$= 0.05, M_0/M_s= 1/4, D'/a = 8)

thickness, while it is not sensitive to variation in bedrock stiffness. Also, frequency ω_{peak} is lower than the resonant frequency ω_L of free-field response, but this is evident only for thin soil layer (D/a = 4) with large embedment (d/a = 2.5), while for thick soil layer (D/a = 8) or small embedment (d/a = 1.5), the two frequencies are difficult to distinguish. The difference of dimensionless peak frequency $\omega_{peak}a/\beta_L$ to dimensionless resonant frequency $\omega_L a/\beta_L$ is listed in Table 2; it is the maximum value between three tunnel mass.

The maximum difference of $\omega_{peak}a/\beta_L$ to $\omega_L a/\beta_L$ is 25.6%, while in the paper by Liang *et al*. (2013a, b) that studies the soil-foundation-superstructure interaction using the model of a rigid foundation with above-ground structures on it, the peak frequency of foundation response is very sensitive to the variation of parameters such as bedrock stiffness, soil-layer thickness and structure mass. The maximum difference can reach nearly 60%. This is because soil-tunnel interaction involves a rigid system while soil-foundation-superstructure interaction involves a flexible system. So the foundation response is influenced strongly by the site dynamic characteristics, and its spectrum is modified essentially, while the influence of site dynamic characteristics on tunnel response is much smaller. If the soil-foundation interaction is considered without superstructure, which is also a rigid system as the soil-tunnel interaction, or the superstructure is rigid enough that the soil-foundation-superstructure interaction approximates a rigid system as the soil-tunnel interaction, the spectrum characteristics

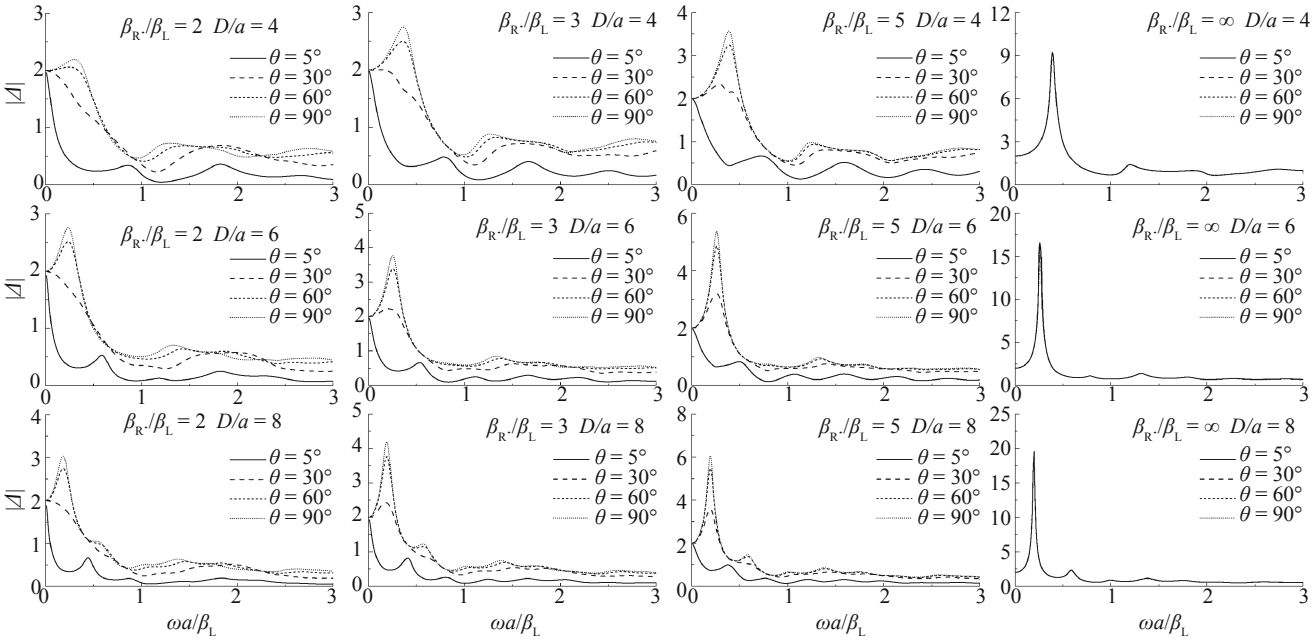

Fig. 5 The spectrum of tunnel displacement versus incident angle θ in layered half-space (d/a = 2, $\rho_R = \rho_L$= 2000 kg/m^3, ξ_L = 0.05, ξ_R = 0.02, M_0/M_s=1/4, D'/a = 8)

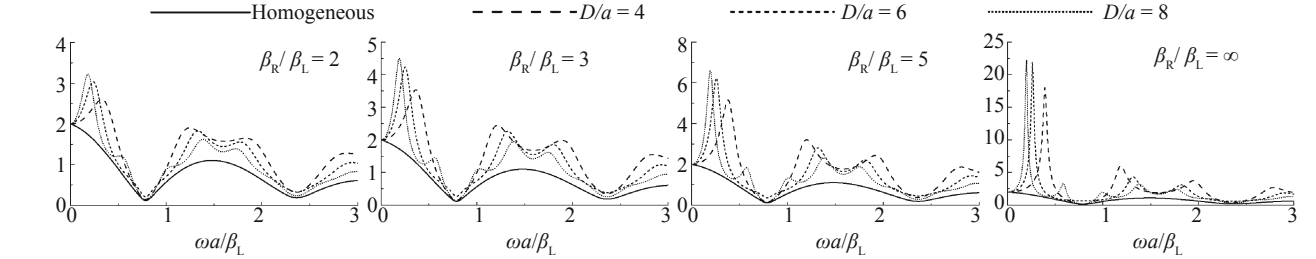

Fig. 6 The spectrum of free-field ground motion at tunnel center for θ = 90° versus different soil-layer thickness (d/a = 2, $\rho_R = \rho_L$= 2000 kg/m^3, D'/a = 8, ξ_L= 0.05 and ξ_R= 0.02 for layered half-space, $\xi_L = \xi_R$= 0.05 for homogeneous half-space)

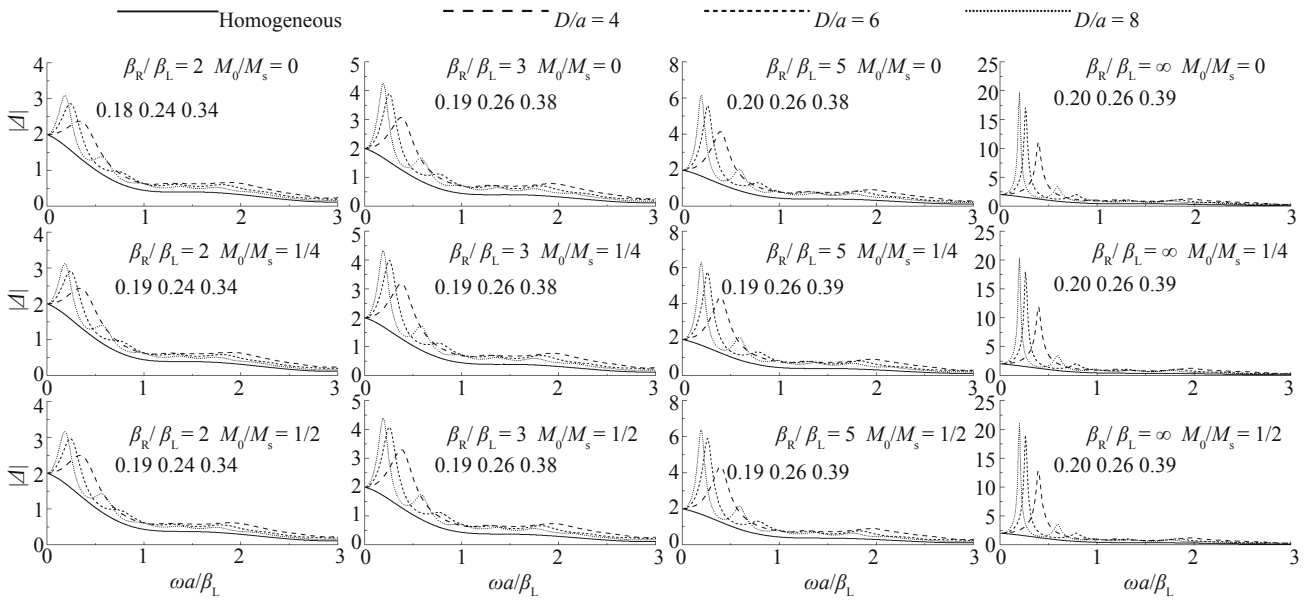

(a) $d/a = 1.5$

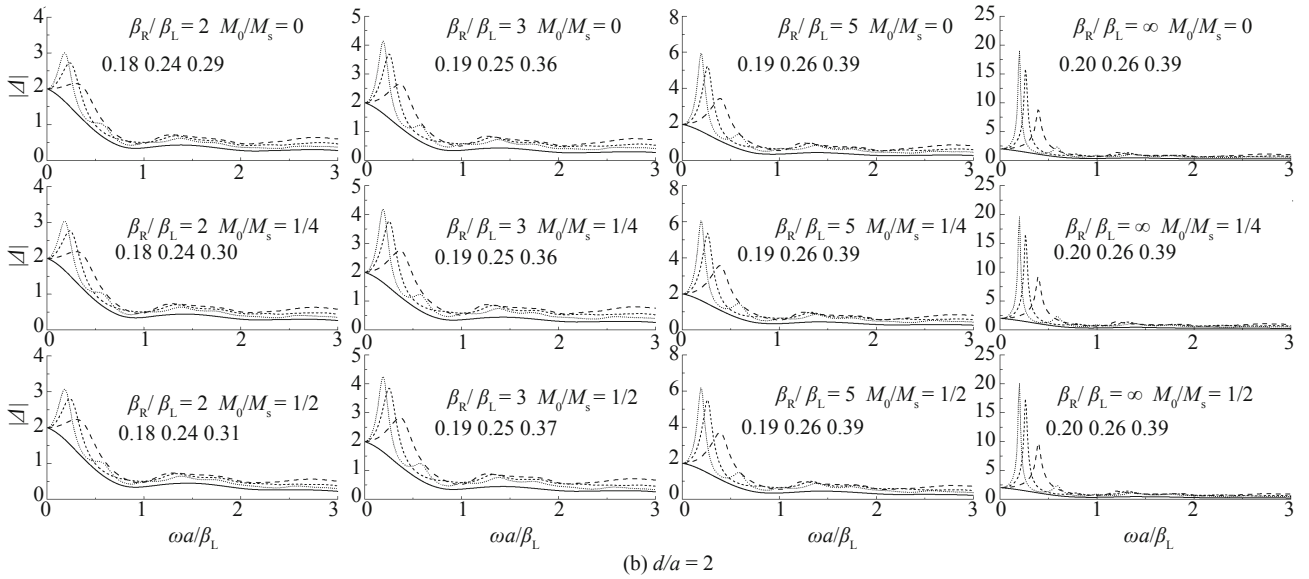

(b) $d/a = 2$

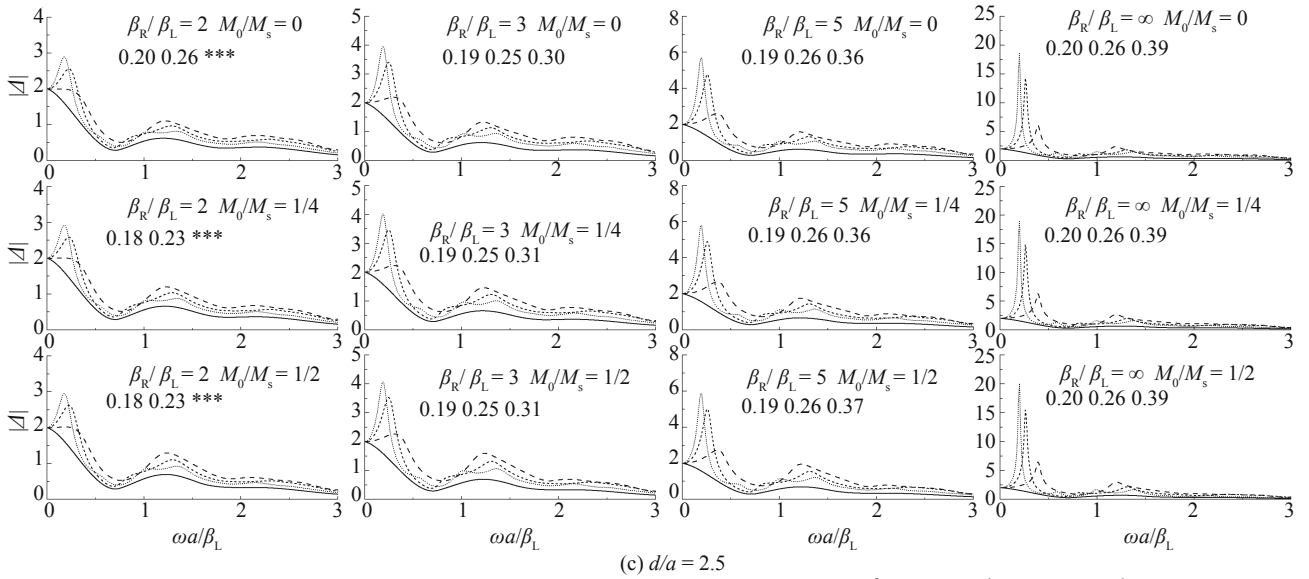

(c) $d/a = 2.5$

Fig. 7 The spectrum of tunnel displacement for vertical incidence ($\rho_R = \rho_L = 2000$ kg/m^3, $D'/a = 8$, $\xi_R = 0.05$ and $\xi_L = 0.02$ for layered half-space, $\xi_R = \xi_L = 0.05$ for homogeneous half-space)

Table 2 Difference of dimensionless peak frequency of tunnel response ($\omega_{peak}a/\beta_L$) to dimensionless resonant frequencies of free-field response ($\omega_L a/\beta_L$) by %

β_R/β_L		2			3			5			∞		
D/a		4	6	8	4	6	8	4	6	8	4	6	8
d/a	1.5	12.8	7.7	10	2.6	0	5	2.6	0	5	0	0	0
	2	25.6	7.7	10	7.7	3.8	5	0	0	5	0	0	0
	2.5	***	11.5	10	23.1	3.8	5	7.7	0	5	0	0	0

of the foundation response would be generally the same as that of the tunnel response; it is not sensitive to these parameters as well.

It is also noticed that the tunnel mass introduces nearly no influence on the spectrum of tunnel response for various half-spaces. The reason is that the tunnel mass itself is small (it is M_0/M_s=0, 1/4 and 1/2 in this paper) and thus the influence of inertia force is limited. It can be concluded that the kinematic interaction dominates in soil-tunnel interaction and the inertia interaction can hardly influence the system when the tunnel mass is small, which results in that its peak frequency is not sensitive to the variation of its mass and that its peak value is much smaller than that of the foundation response in soil-foundation-superstructure interaction

4.3 Analysis in time domain

The tunnel out-of-plane response in the time domain for vertically incident El Centro wave is given in Fig. 8 and for Taft wave in Fig. 9, with a PGA (peak ground acceleration) of 0.1 g. The left part of each sub-figure is the time history of tunnel acceleration with x-axis being the time history by interval 0.02 s and y-axis being the acceleration of 1 g; the right part is the response spectrum of tunnel acceleration with x-axis being the period and y-axis being the maximum acceleration of 1 g. In this section the parameters are: outer radius of the tunnel is a = 5 m, the inner radius is 4m, the embedded depth of d = 10 m, and the tunnel is made of concrete of mass density 2500 kg/m^3. The vertical incident SH wave

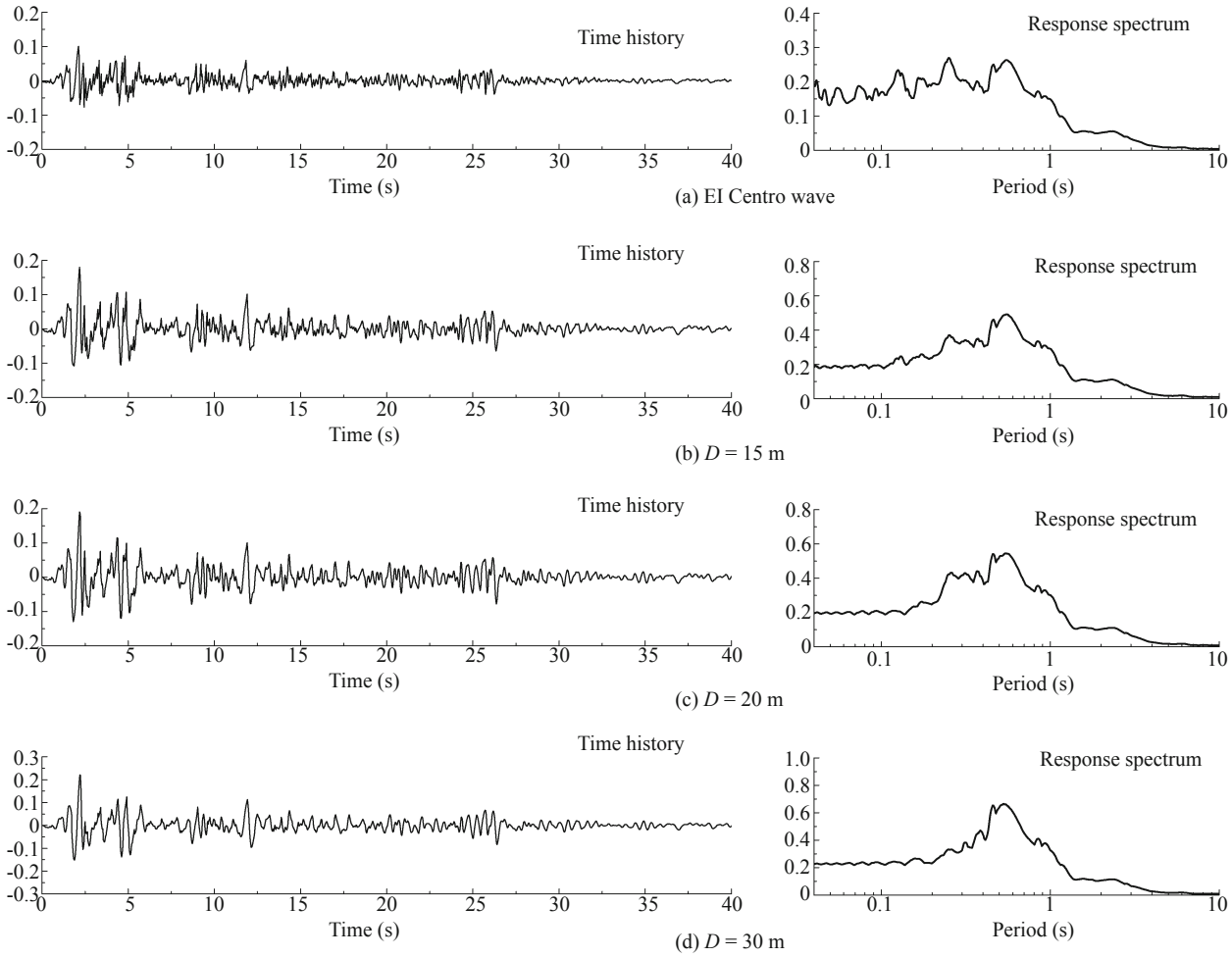

Fig. 8 Time history of acceleration (left) and response spectrum of acceleration (right) of (a) El Centro wave; the tunnel in layered half-space of (b) D = 15 m; (c) D = 20 m; (d) D = 30 m; (e) 40 m; (f) 80 m; (g) in homogeneous half-space for incident El Centro wave from D'= 40 m.

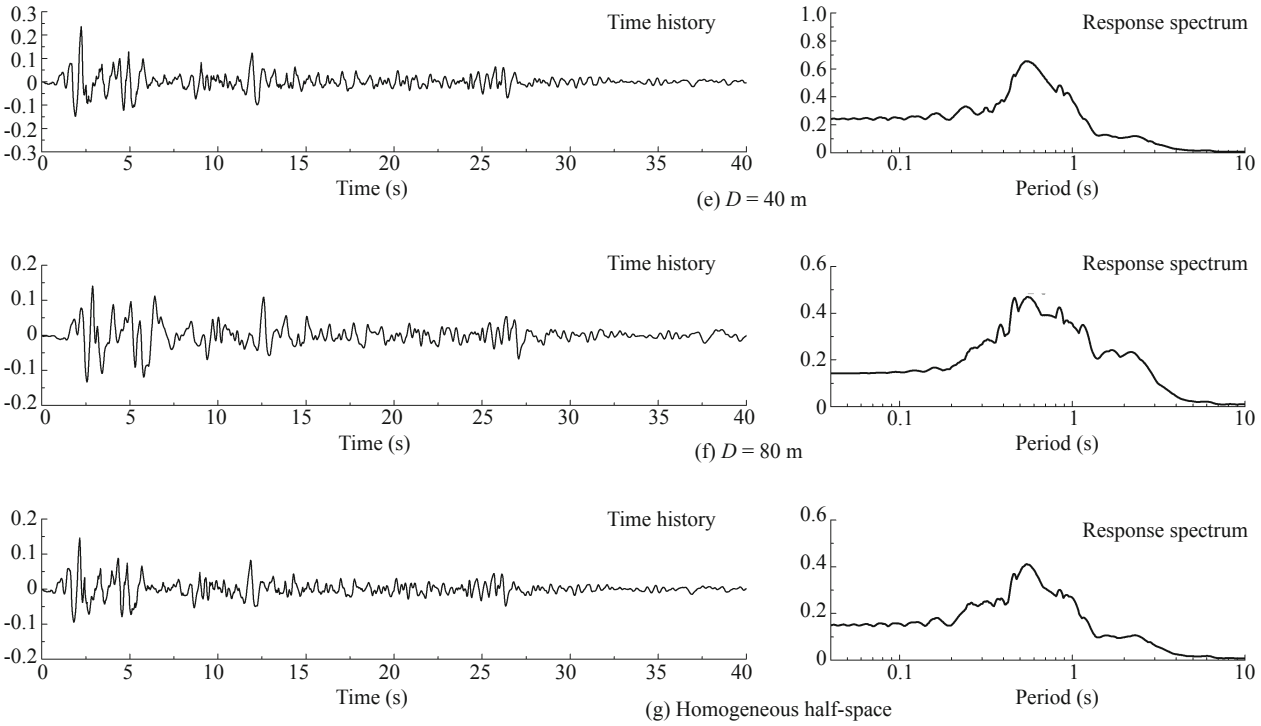

Fig. 8 Continued

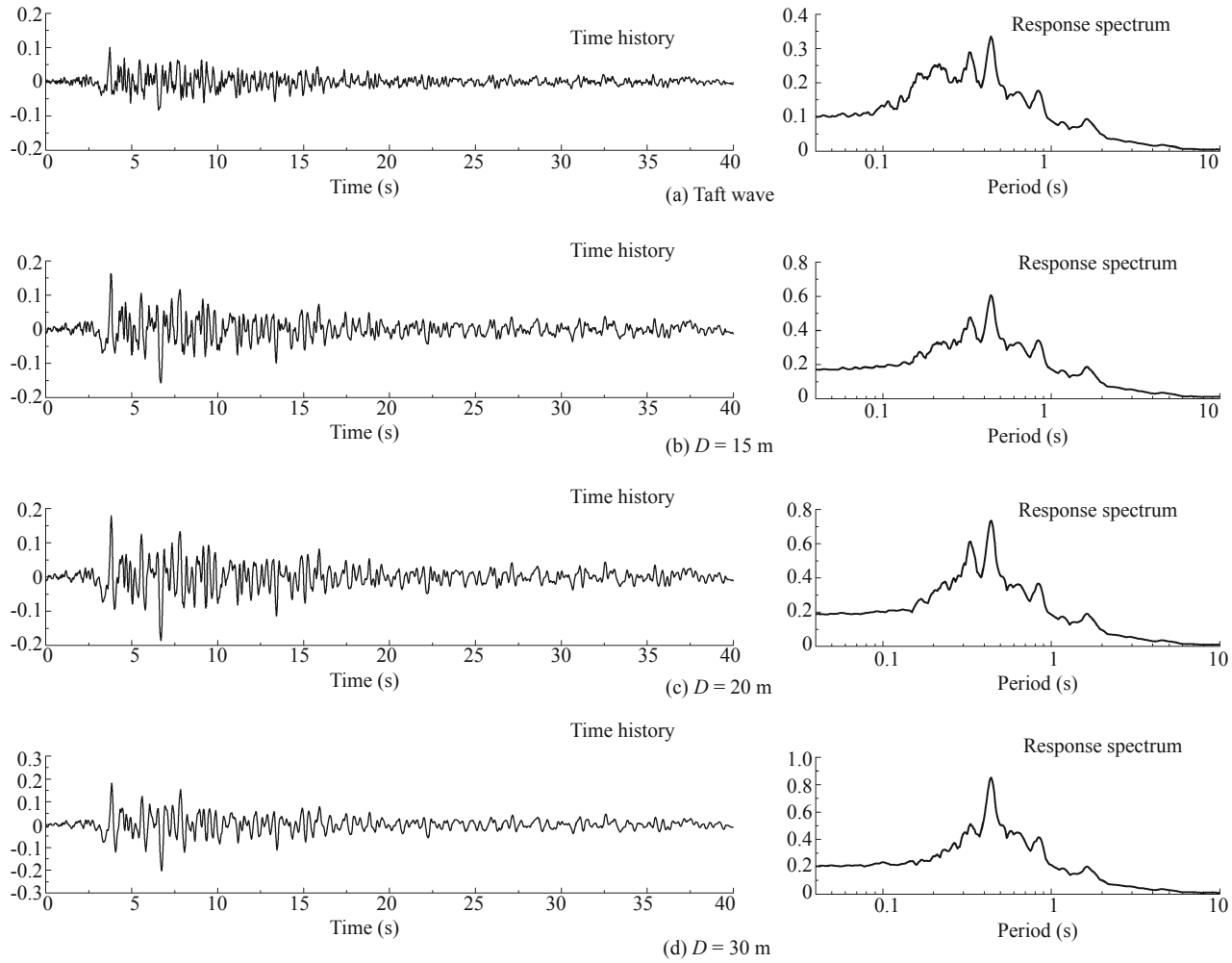

Fig. 9 Time history of acceleration (left) and response spectrum of acceleration (right) of (a) Taft wave; the tunnel in layered half-space of (b) D = 15 m; (c) D = 20 m; (d) D = 30 m; (e) 40 m; (f) 80 m; (g) in homogeneous half-space for incident Taft wave from D' = 40 m.

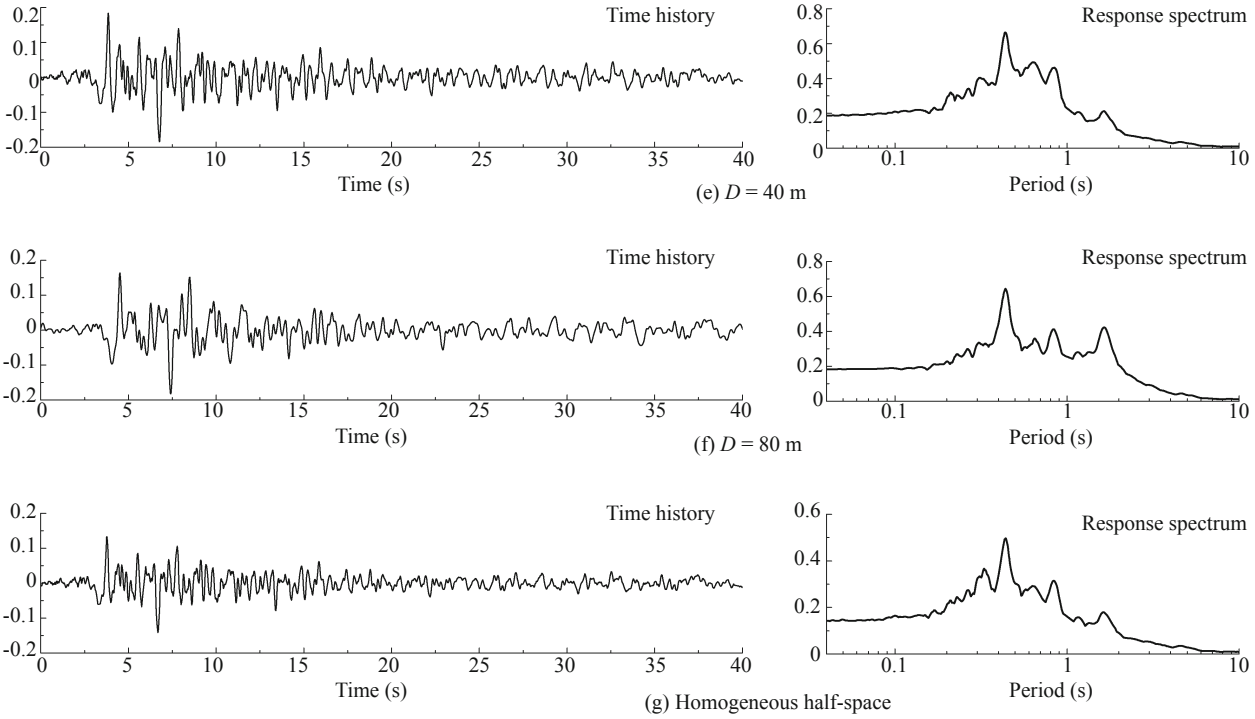

Fig. 9 Continued

comes from depth D' = 40 m. For the layered half-space, the soil-layer thickness is D = 15 m (b), 20 m (c), 30 m (d), 40 m (e) and 80 m (f), which corresponds to D/a = 3, 4, 6, 8 and 16, respectively. Also the soil layer is has a shear wave velocity β_L = 250 m/s, mass density ρ_L = 2000 kg/m^3 and damping ratio ξ_L = 0.02, while the parameters of the bedrock are β_R = 500 m/s, ρ_R = 2000 kg/m^3 and ξ_R = 0.05. The responses in homogeneous half-space are plotted in Fig. 8(g) and 9(g) for comparison, and the homogeneous half-space has shear wave velocity 250 m/s, mass density 2000 kg/m^3 and damping ratio 0.05. Also for comparison, the time history and response spectrum of El Centro wave and Taft wave are also plotted in Fig. 8(a) and 9(a). It is noticed that waves of high frequencies are filtered out for all site conditions in Figs 8(b)−8(g) and 9(b)−9(g).

The calculation of response in time domain was conducted in three steps. First, the time history of earthquake records is converted into frequency domain by Fourier transformation; then the amplification spectrum (tunnel displacement spectrum in Figs. 4 and 5) is calculated at (2048+1) equally spaced frequencies from 0 to 25 Hz, and is multiplied by earthquake record at the corresponding frequency points to obtain the response in frequency domain. Finally this response in frequency domain is converted to time domain by inverse Fourier transformation.

The peak value of time history in Figs. 8(b)-8(g) is 0.180, 0.190, 0.221, 0.236, 0.148 and 0.146, and the peak value of response spectrum is 0.461, 0.542, 0.653, 0.656, 0.466 and 0.411; the peak value of time history in Figs. 9(b)−9(g) is 0.163, 0.185, 0.203, 0.184, 0.182 and 0.141, and the peak value of response spectrum is 0.606, 0.737, 0.853, 0.664, 0.643 and 0.497, respectively. It is observed that the tunnel responses in time domain for the layered half-space are evidently larger than those for the homogeneous half-space. The maximum response in time domain for incident El Centro wave appears for half-space of soil-layer thickness between D =30 m and 40 m, and that for incident Taft wave appears for half-space of D =30 m because the maximum seismic response depends on site dynamic characteristics and spectrum of incident waves.

5 Conclusions

Dynamic soil-tunnel interaction in layered half-space is different from that in homogeneous half-space. The former is more prominent than the latter because the influence of site dynamic characteristics on a tunnel embedded in layered half-space is large, while the homogeneous half-space does not involve these dynamic characteristics of the site.

The mechanism of dynamic soil-tunnel interaction is different from that of dynamic soil-foundation-superstructure interaction because the former is a rigid system and the influence of site dynamic characteristics is relatively smaller, while the latter is a flexible system and the influence of site dynamic characteristics is large. So the difference of the peak frequency of tunnel response to the resonant frequency of the free-field response (the maximum difference is 25.6%) is much smaller than that of foundation response in soil-foundation-superstructure interaction (the maximum difference can reach nearly 60%).

For soil-tunnel interaction, the influence of kinematic interaction is so large that the influence of inertia interaction can hardly be reflected in the dynamic response when the tunnel mass is small. The influence of embedment depth on peak frequency is also very small, but its influence on peak value is relatively evident in the way that the peak value decreases with increasing embedment depth.

Acknowledgement

This study is supported by National Natural Science Foundation of China under grant 51378384 and Key Project of Natural Science Foundation of Tianjin Municipality under Grant 12JCZDJC29000.

References

Balendra T, Thambiratnam DP, Chan GK and Seng LL (1984), "Dynamic Response of Twin Circular Tunnels due to Incident SH-waves," *Earthquake Engineering and Structural Dynamics*, **12**: 181−201.

De Barros FCP and Luco JE (1994), "Seismic Response of a Cylindrical Shell Embedded in a Layered Viscoelastic Half-space. II: Validation and Numerical Results," *Earthquake Engineering and Structural Dynamics*, **23**: 569−580.

Fu Jia, Liang Jianwen and Du Jinjin (2016), "Analytical Solution of Dynamic Soil-tunnel Interaction for Incident Plane SH Wave," *Chinese Journal of Geotechnical Engineering*, **38**(4): 588–598. (in Chinese)

Hasheminejad SM and Avazmohammadi R (2008), "Dynamic Stress Concentrations in Lined Twin Tunnels within Fluid-saturated Soil," *Journal of Engineering Mechanics*, ASCE, **134**: 542−554.

Hatzigeorgiou GD and Beskos DE (2010), "Soil-structure Interaction Effects on Seismic Inelastic Analysis of 3-D Tunnels," *Soil Dynamics and Earthquake Engineering*, **30**: 851−861.

Lee VW and Trifunac MD (1979), "Response of Tunnels to Incident SH-waves," *Journal of the Engineering Mechanics Division*, ASCE, **105**: 643−659.

Liang J, Fu J, Todorovska MI and Trifunac MD (2013a), "Effects of the Site Dynamic Characteristics on Soil-structure Interaction (I): Incident SH waves," *Soil Dynamics and Earthquake Engineering*, **44**: 27–37.

Liang J. Fu J, Todorovska MI and Trifunac MD (2013b), "Effects of the Site Dynamic Characteristics on Soil-structure Interaction (II): Incident P and SV Waves," *Soil Dynamics and Earthquake Engineering*, **51**: 58−76.

Liang J, Ji X and Lee VW (2005a), "Effects of an Undergrond Lined Tunnel on Ground Motion (I): Series Solution," *Rock and Soil Mechanics*, **26**(4): 520−524. (in Chinese)

Liang J, Ji X and Lee VW (2005b), "Effects of an Undergrond Lined Tunnel on Ground Motion (II): Numerical Results," *Rock and Soil Mechanics*, **26**(5): 687−692. (in Chinese)

Luco JE (1986), "On the Relation between Radiataion and Scattering Problems for Foundations Embedded in an Elastic Half-space," *Soil Dynamics and Earthquake Engineering*, **5**(2): 97–101.

Luco JE and De Barros FCP (1994), "Seismic Response of a Cylindrical Shell Embedded in a Layered Viscoelastic Half-space. I: Formulation," *Earthquake Engineering and Structural Dynamics*, **23**: 553−567.

Luco JE and Wong HL (1982), "Response of Structures to Nonvertically Incident Seismic Waves," *Bulletin of the Seismological Society of America*, **72**(1): 275–302.

Parvanova SL, Dineva PS, Manolis GD and Wuttke F (2014), "Seismic Response of Lined Tunnels in the Half-plane with Surface Topography," *Bulletin of Earthquake Engineering*, **12**: 981−1005.

Pitilakis K, Tsinidis G, Leanza A and Maugeri M (2014), "Seismic Behaviour of Circular Tunnels Accounting for Above Ground Structures Interaction Effects," *Soil Dynamics and Earthquake Engineering*, **67**: 1−15.

Wolf JP (1985), *Dynamic Soil-structure Interaction*, Prentice-Hall, Englewood Cliffs.

Wong KC, Shah AH and Datta SK (1985), "Dynamic Stresses and Displacements in a Buried Tunnel," *Journal of the Engineering Mechanics Division*, ASCE, **111**(2): 218−234.

Appendix: Solution by wave function expansion method (Fu *et al*., 2016)

The displacement field of the half-space with a rigid tunnel embedded in is

$$w(r_1,\theta_1)=w_1^{\mathrm{i}}(r_1,\theta_1)+w_2^{\mathrm{i}}(r_1,\theta_1)+w_1^{\mathrm{r}}(r_1,\theta_1)+w_2^{\mathrm{r}}(r_1,\theta_1) \tag{A1}$$

in which

$$w_1^{\mathrm{i}}(r_1,\theta_1)=\sum_{m=0}^{\infty}\varepsilon_m(-\mathrm{i})^m\mathrm{J}_m(kr_1)\left(\cos m\theta\cos m\theta_1+\sin m\theta\sin m\theta_1\right) \tag{A2a}$$

$$w_2^{\mathrm{i}}(r_1,\theta_1)=\exp(-2\mathrm{i}kd\cos\theta)\sum_{m=0}^{\infty}\varepsilon_m\mathrm{i}^m\mathrm{J}_m(kr_1)\cdot\left(\cos m\theta\cos m\theta_1-\sin m\theta\sin m\theta_1\right) \tag{A2b}$$

$$w_1^{\mathrm{r}}(r_1,\theta_1)=\sum_{m=0}^{\infty}\mathrm{H}_m^{(2)}(kr_1)\left(A_m\cos m\theta_1+B_m\sin m\theta_1\right) \tag{A2c}$$

$$w_2^{s}(r_2,\theta_2)=\sum_{n=0}^{+\infty}\mathrm{H}_n^{(2)}(kr_2)\left(A_n\cos n\theta_2+B_n\sin n\theta_2\right) \tag{A2d}$$

Equation (A2d) can be transformed from coordinates (r_2,θ_2) to coordinates (r_1,θ_1) by Graf Addition Theorem

$$w_2^r(r_1,\theta_1)=\sum_{m=0}^{\infty}\frac{\varepsilon_m}{2}\mathrm{J}_m(kr_1)\sum_{n=0}^{\infty}\left\{A_nP_m^n(2kd)\cos m\theta_1+B_nQ_m^n(2kd)\sin m\theta_1\right\} \tag{A3}$$

The details on Eqs. (A1)−(A3) can be found in Lee and Trifunac (1979). The equilibrium equation of the rigid tunnel is

$$a\mu\int_0^{2\pi}\frac{\partial w}{\partial r_1}\Big|_{r_1=a}d\theta_1=-\omega^2M_0\,w\big|_{r_1=a} \tag{A4}$$

which can lead to a set of infinite equations

$$\left[\mathrm{H}_0^{(2)}(ka)+\frac{2}{ka}\frac{M_\mathrm{s}}{M_0}\mathrm{H}_0^{(2)'}(ka)\right]A_0+\left[\mathrm{J}_0(ka)+\frac{2}{ka}\frac{M_\mathrm{s}}{M_0}\mathrm{J}_0'(ka)\right]\sum_{n=0}^{\infty}A_n\mathrm{H}_n^{(2)}(2kd)=-\frac{2}{ka}\frac{M_\mathrm{s}}{M_0}\mathrm{J}_0'(ka)-\frac{2}{ka}\frac{M_\mathrm{s}}{M_0}\exp(-2\mathrm{i}kd\cos\theta)\mathrm{J}_0'(ka)-\mathrm{J}_0(ka)-\exp(-2\mathrm{i}kd\cos\theta)\mathrm{J}_0(ka)\qquad m=0 \tag{A5a}$$

$$A_m\frac{\mathrm{H}_m^{(2)}(ka)}{\mathrm{J}_m(ka)}+\sum_{n=0}^{\infty}A_nP_m^n(2kd)=-2(-\mathrm{i})^m\cos m\theta-2\exp(-2\mathrm{i}kd\cos\theta)\mathrm{i}^m\cos m\theta\qquad m=1,\ 2,\ 3\ldots \tag{A5b}$$

$$B_m\frac{\mathrm{H}_m^{(2)}(ka)}{\mathrm{J}_m(ka)}+\sum_{n=0}^{\infty}B_nQ_m^n(2kd)=2\exp(-2\mathrm{i}kd\cos\theta)\mathrm{i}^m\sin m\theta-2(-\mathrm{i})^m\sin m\theta\qquad m=1,\ 2,\ 3\ldots \tag{A5c}$$

in which M_s is mass of the soil replaced by the tunnel. The unknowns A_m and B_m can be solved by truncating (A5) into a set of finite equations, then the tunnel displacement is

$$\Delta=\mathrm{J}_0(ka)+\exp(-2\mathrm{i}kd\cos\theta)\mathrm{J}_0(ka)+A_0\mathrm{H}_0^{(2)}(ka)+\mathrm{J}_0(ka)\sum_{n=0}^{\infty}A_n\mathrm{H}_n^{(2)}(2kd) \tag{A6}$$

The accuracy of the method can be justified by introducing Eqs. (A2) into (A4) to inspect the boundary condition.